Biosensors and Bioelectronics 158 (2020) 112179

Contents lists available at ScienceDirect

Biosensors and Bioelectronics

journal homepage: http://www.elsevier.com/locate/bios

Three–dimensional donor–acceptor–type photoactive material/conducting polyaniline hydrogel complex for sensitive photocathodic enzymatic bioanalysis

Min Qing, Sheng Liang Chen, Lei Han, Yu Zhu Yang, Hong Qun Luo **, Nian Bing Li *

Key Laboratory of Eco–Environments in Three Gorges Reservoir Region (Ministry of Education), School of Chemistry and Chemical Engineering, Southwest University, Chongqing, 400715, PR China

ARTICLE INFO

Keywords:
Donor–acceptor–type photoactive material
Polyaniline hydrogel
Photoelectrochemical enzymatic bioanalysis

ABSTRACT

Herein, an innovative photocathodic enzymatic biosensor is proposed with poly {4,8-bis[5-(2-ethylhexyl)thiophen-2-yl]-benzo[1,2-b:4,5-b']dithiophene-2,6-diyl-alt-3-fluoro-2-[(2-ethylhexyl)carbonyl]thieno[3,4-b]thiophene-4,6-diyl} (PTB7–Th) as donor–acceptor–type photoactive material and three–dimensional (3D) polyaniline hydrogels (PAniHs) as both electron transfer layer and biomolecule carrier. Based on the enhancement effect of PAniHs on the charge separation and electron transfer of PTB7–Th and the competitive consumption of dissolved oxygen (O_2) between the xanthine oxidase (XOD)–guanine catalytic reaction and O_2–sensitive PTB7–Th/PAniHs, the proposed photocathodic enzymatic biosensor has been demonstrated to detect guanine with the advantages of low limit of detection (0.02 μM), wide linear range (from 0.1 to 80 μM), simple and convenient preparation process, satisfactory stability, and photochemical signal amplification independent of any exogenous electron donor/acceptor or sensitizer. Remarkably, the proposed photocathodic enzymatic biosensor can not only be extended to other aerobic enzymatic bioanalyses, but also pave a horizon for the application of environmentally friendly conductive hydrogel materials in photoelectrochemical bioanalysis.

1. Introduction

With its unique merits of low background noise, high sensitivity, simplification and miniaturization, photoelectrochemical biosensor (PEC) has stimulated keen interest to design and engineer sensing platforms with applications ranging from environmental analysis to clinical diagnosis, and relevant field (Dong et al., 2020; Wang et al., 2019; Zang et al., 2017; Zhao et al., 2017). Amounts of ingenious strategies have been reported to improve the efficiency of photoelectric conversion by directly injecting the electron donor/acceptor (D/A) of photoactive materials into electrolyte (Wei et al., 2018, 2019; Xue et al., 2019; Zhang et al., 2018a), or in situ generating the electron D/A on the surface of photoactive materials (Shen et al., 2015; Ye et al., 2016; Zang et al., 2014). Despite their impressive performance, the photoelectric conversion efficiency is limited by intermolecular electron transfer to some extent. Comparatively, donor–acceptor–type photoactive materials integrate electron-deficient monomer and electron-rich monomer into one molecule, possess intramolecular electron transfer process, facilitate electron transfer rate, and enhance photoelectric conversion efficiency. These features have experienced soaring popularity (Cho et al., 2012; Liao et al., 2013; Sayresmith et al., 2019). Unfortunately, the reported donor–acceptor–type photoactive material lacks modifiable chemical groups, making it challenge with efficient immobilization and functionalization methods in further applications. To overcome these drawbacks, some strategies, such as packaging donor–acceptor–type photoactive material and its sensitizer with microcapsule or coating a layer of gold nanoparticles on the surface of donor–acceptor–type photoactive material via electrochemical deposition, have been implemented to expand its applications in PEC (Li et al., 2018; Zheng et al., 2016). Current immobilization and functionalization strategies suffer, however, from complicated and time−consuming preparation procedure, high cost, as well as limited loading amounts on account of restricted two–dimensional (2D) planar space, impeding the sensitivity and practicality of the PEC biosensor. More importantly, the bulk heterostructures limit the accessibility of the electrolyte to the internal photoactive sites, which is adverse to diffusion kinetics for hydrosoluble

* Corresponding author.
** Corresponding author.
E-mail addresses: luohq@swu.edu.cn (H.Q. Luo), linb@swu.edu.cn (N.B. Li).

https://doi.org/10.1016/j.bios.2020.112179
Received 2 March 2020; Received in revised form 24 March 2020; Accepted 26 March 2020
Available online 27 March 2020

matter and electrons, resulting in reduced PEC response (Fan et al., 2015; Hao et al., 2017; Qiu et al., 2018; Shi et al., 2018). Therefore, advance in designing a multifunctional carrier for photoactive materials and biomolecules with multiple properties including hierarchically porous structure, effective and robust loading capability, excellent conductivity, as well as convenient preparation steps, is desirable.

Three–dimensional (3D) polyaniline hydrogels (PAniHs), synergizing the unique properties including but not limited to outstanding conductivity, hierarchically porous structure, as well as high permeability to molecules, may offer proper synergic species for photoactive materials (Jiang et al., 2016; Pan et al., 2012). In addition, the 3D PAniHs reveal similarities with native tissues, making them as suitable matrix for biomolecules adhesion (Li et al., 2015; Zhang et al., 2019). Inspired by the outstanding performance of 3D PAniHs, herein, we designed 3D PAniHs as the carrier for both donor–acceptor–type photoactive material and biomolecule for the first time, which not only simplify the preparation procedure and greatly enhance the molecules−loading amounts, but also facilitate the diffusion kinetics of hydrosoluble matter and electrons compared with the bulk heterostructures, thus greatly enhancing the PEC signal.

In the present work, as a proof–of concept, we constructed a cathodic PEC biosensor based on donor–acceptor–type photoactive material–modified polyaniline hydrogels (PTB7–Th/PAniHs) for detection of guanine. As depicted in Scheme 1, the PAniHs are assembled onto the surface of glassy carbon electrode (GCE) by fast polyreaction of aniline monomer, phytic acid, and polymerization initiator within 3 min. The PTB7–Th/PAniHs can be obtained by directly embedding PTB7–Th into the hydrogels skeleton, resulting in a high initial photocurrent signal without any exogenous sensitizer or electron D/A for photocurrent amplification. The significantly enhanced initial photocurrent signal is attributed to the following reasons: first, enhanced electron diffusivity and molecule permeability due to the solvated surfaces and highly porous network of the hydrophilic hydrogels; second, the greatly increased loading amounts of photoactive material due to the large specific surface area of 3D hydrogels architecture. The enzyme immobilization is, with xanthine oxidase (XOD) as a model biocatalyst, achieved by classic glutaraldehyde (GA) reaction between the amino groups on the framework of hydrogel and the amino groups of the biomolecules (Li et al., 2015). Guanine, one of the critical nucleobases in DNA, RNA and other biological species, participates in a variety of biochemical processes. Abnormal guanine level in organism may obstruct the metabolic activity of enzymes, indicate the degree of DNA oxidative damage, and reflect some genetic diseases, which is significant for clinical medicine and biological science (Fu et al., 2019; Gao et al., 2014; Ng and Khor, 2017). In the presence of guanine, XOD will catalyze its oxidation to uric acid, resulting in the consumption of dissolved oxygen (Xu et al., 2019b). Since the dissolved oxygen as the electron accepter of PTB7–Th/PAniHs is consumed by the enzyme–biocatalytic process, the initial photocurrent is effectively decreased. Consequently, the proposed PEC platform achieved guanine detection with high accuracy and sensitivity. The proposed PEC strategy not only provided a novel paradigm for improving the photoelectric conversion efficiency of photoactive material, but also established a foundation for the utilization of environmental–friendly materials in the PEC enzymatic bioanalysis.

2. Experimental

2.1. Chemicals

Poly {4,8–bis[5–(2–ethylhexyl)thiophen–2–yl]–benzo[1,2–b:4,5–b′] dithiophene– 2,6–diyl–alt–3–fluoro–2–[(2–ethylhexyl)carbonyl]thieno [3,4–b]thiophene–4,6–diyl} was purchased from Luminescence Technology Co., Ltd. (Taiwan, China). Aniline (analytical reagent grade, 99.5%), ascorbic acid (AA) and dichloromethane were purchased from Kelong Chemicals Ins. (Chengdu, China). Phytic acid (50%, w/w in water) was bought from Sigma−Aldrich Co., Ltd. (Shanghai, China). Ammonium persulfate (ACS grade, ≥98.0%) and xanthine oxidase (XOD, 5 U) were supplied from Sangon Biotech. Co., Ltd. (Shanghai, China). Histidine, arginine, dopamine (DA) and guanine were obtained from Aladdin Chemistry Co., Ltd. (Shanghai, China). In the experiment, deionized water was used with a resistance of 18.2 MΩ cm. Stock solution of guanine (20 mM, 100 mL) was prepared by dissolving guanine powder with sodium hydroxide (0.1 M), and then stored at 4 °C for further use.

2.2. Apparatus

Morphology and the corresponding energy dispersive X−ray spectroscopy (EDS) elemental mapping of samples were characterized by field emission scanning electron microscopy (FE−SEM, JSM−7800F, JEOL, Japan). The UV−vis diffuse reflectance spectrum was studied on a spectrophotometer (Agilent Cary 5000, Agilent Technologies Inc., Malaysia). The chemical bond and functional group of samples were tested by fourier transform infrared spectrometer (FTIR, Nicolet iS10, Nicolet Co., Ltd., U.S.A.). The electronic structure and compositions of samples were analyzed by X−ray photoelectron spectrometer (XPS,

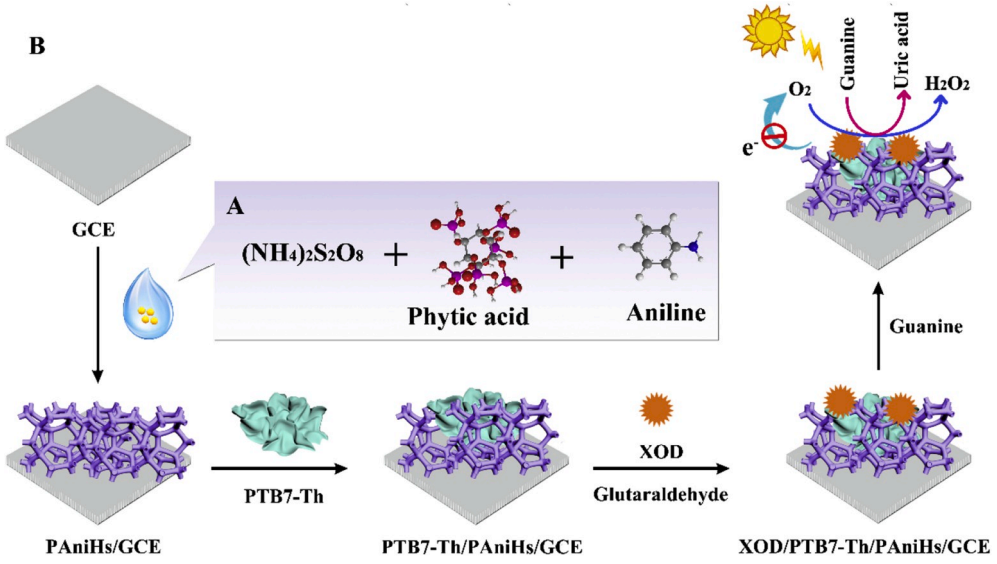

Scheme 1. Schematic illustration of 3D PTB7–Th/PAniHs–Based Photocathodic Enzymatic Bioanalysis.

Thermo Scientific K−Alpha, Thermo Fisher Scientific Inc., U.S.A.). CHI 660E electrochemical workstation (Chenhua, Shanghai Chenhua Instruments Co., Ltd., China) was applied for electrochemical and PEC measurements, in which PEC10W−2 (Guangzhou Benguang Technology Co., Ltd., China) was configured throughout the PEC measurements process for visible−light irradiation. A three−electrode system, containing a glassy carbon electrode (GCE, Φ = 3 mm) as the working electrode, Ag/AgCl as the reference electrode and a platinum wire as the auxiliary electrode, was used through the experiment.

2.3. Fabrication and measurement of the PEC sensing platform

First, polyaniline hydrogels modified electrode (PAniHs/GCE) was prepared referring to the literature (Li et al., 2015). Subsequently, PTB7–Th (5 μL, 1 mg mL^{-1}) was pipetted onto the PAniHs/GCE and coated onto the surface of PAniHs due to its good film–forming property. Because PAniHs have abundant amino groups on the framework of the PAni, Schiff base reaction was adopted for immobilizing the enzyme on the electrode. The XOD (0.5 mg mL^{-1}, 5 μL) and glutaraldehyde (1%, 5 μL) were dropped onto the modified electrode (PTB7–Th/PAniHs/GCE), and then reacted for 30 min at 25 °C. After washing with Tris–HCl buffer (10 mM, pH 7.4), the XOD/PTB7–Th/PAniHs/GCE was stored at 4 °C before use. For the analysis of guanine, the XOD/PTB7–Th/PAniHs/GCE was immersed into 7 mL of Tris–HCl buffer (10 mM, pH 7.4) containing various concentrations of guanine. After incubation for 25 min, the photocurrent response was monitored by the CHI 660E electrochemical workstation (constant potential of 0 V, *vs* Ag/AgCl, in air) equipped with a LED lamp (light window diameter is 12 mm, optical output power is 5400 mW, and off-on-off switch is set to 10-15-10 s). For the nitrogen interference test, the other measuring conditions remain unchanged except sweeping away the oxygen in the buffer with the nitrogen bubble.

3. Results and discussion

3.1. Characterization of PAniHs and PTB7–Th/PAniHs

Fig. 1A describes that the PAniHs were assembled by polyreaction of phytic acid and PAni. PAni chains were crosslinked with phytic acid molecule on account of the protonation of nitrogen groups on PAni, leading to the formation of mesh–like network. As shown in Fig. 1B, dark green PAniHs form in a glass vial. Scanning electron microscopy (SEM) image (Fig. 1C) indicates that the dehydrated PAniHs showed a 3D porous structure and was composed of coral–like nanofibers with a uniform diameter of about 100 nm. Moreover, the magnified SEM image reveals that PAniHs have micron sized pores (Fig. 1D), which are favorable for embedding guest molecules. The corresponding elemental mapping images of PAniHs demonstrate the evenly spaced distribution of C, N, and O in its skeleton (Fig. 1F). Fig. 1E reveals that PTB7–Th was coated on the porous PAniHs, indicating that PTB7–Th possesses excellent ductility and film–forming property.

The UV–vis diffuse reflectance spectra were performed to study optical absorption properties of PAniHs, PTB7–Th, and PTB7–Th/PAniHs (Fig. 2A). The PTB7–Th shows strong absorption ranging from 500 nm to longer wavelength, verifying its outstanding photoelectric conversion efficiency. As depicted from the absorption peak of the PAniHs, the poor photoabsorption locates at about 450 nm, which confirms the doped emeraldine state (Pan et al., 2012). After PAniHs was modified with PTB7–Th, the range of absorption peak of PTB7–Th (500–760 nm) shifted positively ca. 25 nm, indicating that PAniHs facilitate the light absorption of PTB7–Th. According to the Tauc plots of PTB7–Th and PTB7–Th/PAniHs complex (Fig. S1), the values of bandgap energy for the as–prepared PTB7–Th and PTB7–Th/PAniHs are estimated to be 1.62 and 1.51 eV, respectively. Compared with PTB7–Th, the decreased bandgap energy in PTB7–Th/PAniHs demonstrates that PAniHs can boost PEC activity of PTB7–Th. Also, the elemental components of

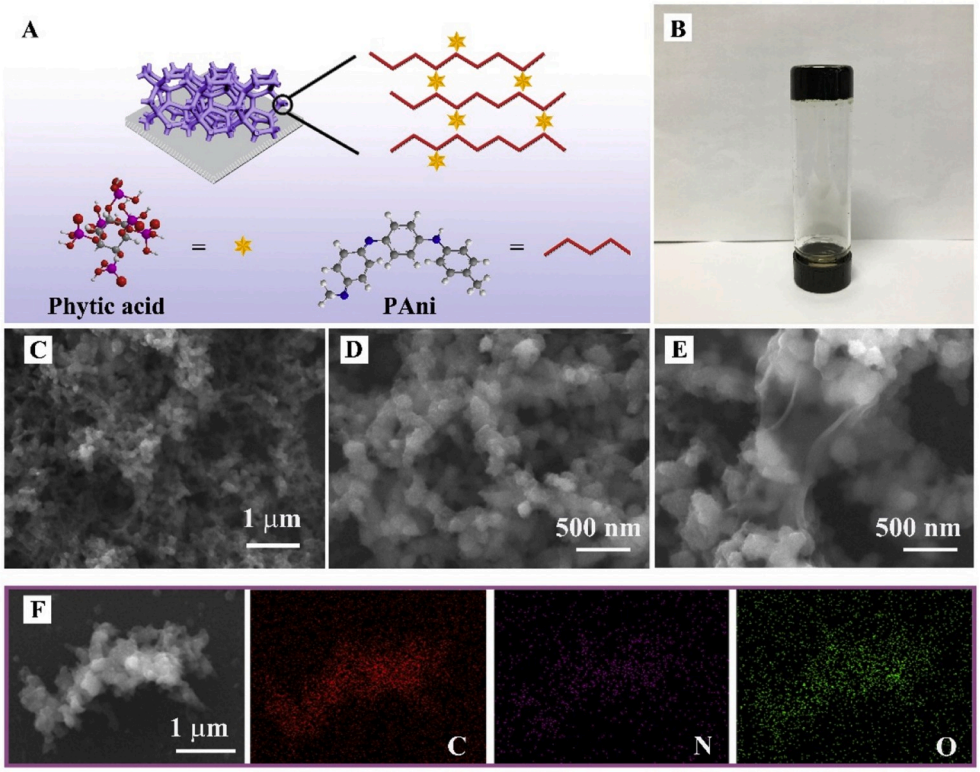

Fig. 1. (A) Diagrammatic sketch of synthesis of 3D PAniHs. (B) Photograph of the PAniHs synthesized in a glass vial. (C) SEM image of the dehydrated PAniHs. D) A higher magnification SEM image of the dehydrated PAniHs. (E) A higher magnification SEM image PAniHs with embedded PTB7–Th. (F) SEM and corresponding elemental mapping images of C, N, and O for PAniHs.

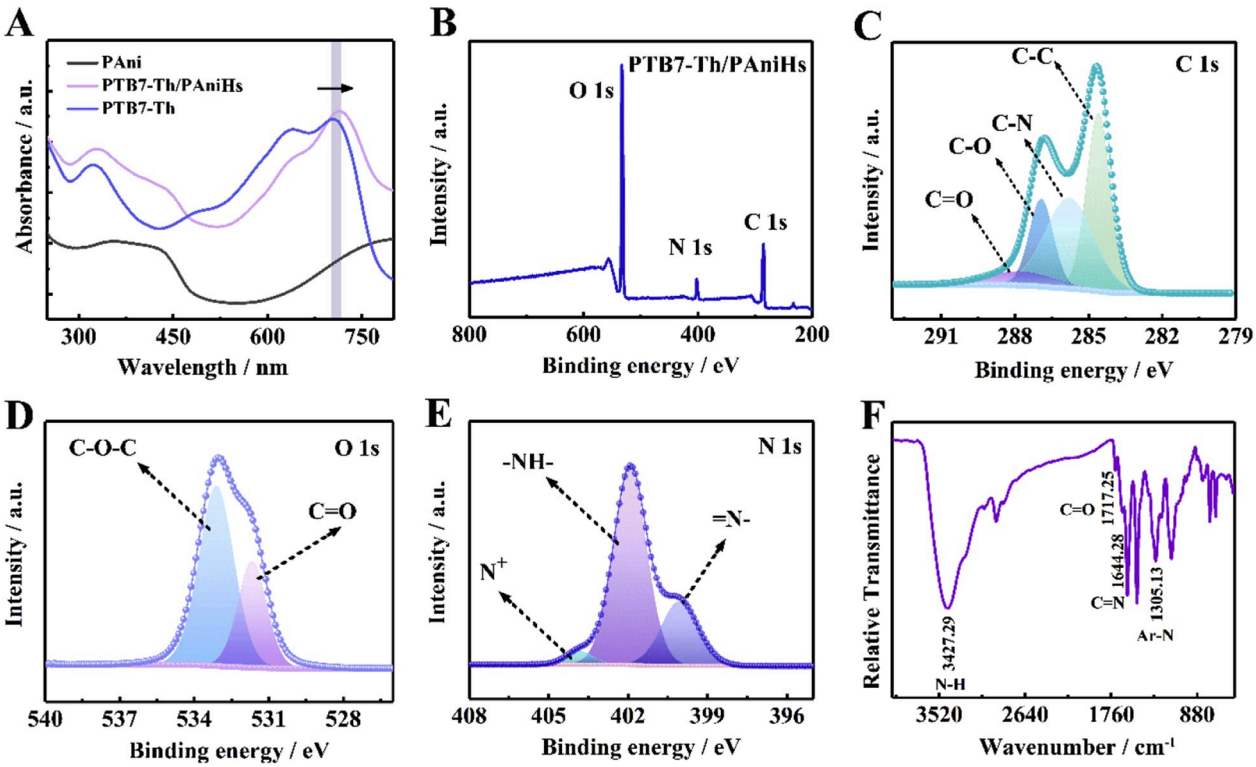

Fig. 2. (A) UV–vis diffuse reflectance spectra of PAniHs, PTB7–Th, and PTB7–Th/PAniHs. XPS analysis for (B) full survey spectrum of PTB7–Th/PAniHs, (C) XPS narrow−scan spectra of PTB7–Th/PAniHs for C 1s, (D) O 1s, and (E) N 1s. (F) FT–IR spectra of XOD/PAniHs.

PTB7–Th/PAniHs complex were analyzed by X–ray photoelectron spectroscopy (XPS). Fig. 2B presents the full survey spectrum, demonstrating that the zigzag region is nearly pure PTB7–Th/PAniHs complex. As depicted in Fig. 2C, the major peak line of C 1s could be split into four main peak lines, in which the maximal peak at 284.60 eV corresponds to the C–C bond. The peak at 285.79 eV was caused by C–N and C═N bonds, and the peak at 286.93 eV was the characteristic peak of C–O bond. The peak at 287.78 eV was assigned to the C═O bond, attributing to the –C═O in the carboxylic group (−COOH) of the PTB7–Th (Vilian et al., 2019; Xu et al., 2019a). Also, the core peak line of O 1s shows two main peaks at 531.67 and 533.11 eV (Fig. 2D), corresponding to the C═O and C–O–C bond, which confirms the presence of PTB7–Th (Jiang et al., 2016). As shown in Fig. 2E, the major peak line of N 1s can be decomposed into three peak lines, in which the peaks of the quinoid di−imine and benzenoid diamine nitrogen located at 400.05 and 401.93 eV, respectively. The peak located at 403.84 eV is relating to positively charged nitrogen (Wu et al., 2006). Thus, these results verified the successful synthesis of PTB7–Th/PAniHs complex.

Furthermore, the Schiff base reaction between PAniHs and enzyme was determined by Fourier transform infrared (FT−IR) spectroscopy (Fig. 2F). The peaks at 1305.13 cm^{-1} and 3427.29 cm^{-1} belong to the absorption of Ar–N and N–H bonds in PAniHs molecule, respectively. The peak located at 1717.25 cm^{-1} represents the C═O bond. The characteristic absorption at 1644.28 cm^{-1} attributes to the stretching vibration of covalent C═N bond (Li et al., 2015), demonstrating the successfully immobilized enzymes on the hydrogel.

3.2. PEC characterization of the modified biosensor

For verifying the stepwise modification process and the feasibility of cathodic PEC biosensor, the PEC responses were recorded in the Tris–HCl buffer. From Fig. 3A, the PAniHs modified biosensor (PAniHs/GCE) exhibits a weak PEC response. When the PTB7–Th was coated on the PAniHs/GCE, an obviously increased PEC response was obtained due to the enhancement effect of PAniHs on PTB7–Th. After further modification of XOD, the PEC response was decreased on account of steric–hindrance effect of the protein biomolecules (Mahshid et al., 2015; Tu et al., 2016). After incubation with guanine, a decreased PEC response was observed, attributing to the fact that the dissolved oxygen as the electron accepter of PTB7–Th/PAniHs was consumed by the XOD–guanine catalytic reaction. All of the results demonstrated the successful construction of the biosensor.

3.3. Mechanism of electron transfer

First, for assessing whether the PAniHs could serve as an effective hole transfer material, the open circuit potential (OCP) test was conducted under dark and illumination (Fig. S2). Upon illumination, the OCP shifted to a more positive potential, while decreased slowly in the dark condition. This phenomenon indicated that holes generated from PAniHs can be transferred to PTB7–Th in the proposed photocathode (Li et al., 2016). Moreover, nitrogen (N_2) interference assay was performed to demonstrate that the PTB7–Th/PAniHs photocathode was O_2–sensitive (Fig. S3). Therefore, the PTB7–Th/PAniHs cathodic PEC enzymatic bioanalysis was constructed (Fig. 3B). Under visible–light irradiation, the photoexcited electrons in PTB7–Th molecule were transferred from the donor unit to the acceptor unit, and then transferred to the conduction band (CB) of PAniHs because of the suitable energy band matching. Importantly, the unique structure of the PAniHs facilitates the fast charge separation and electron transfer (Lee et al., 2006). Since the photogenerated electrons were accepted by the dissolved oxygen in the electrolyte, a significant cathodic photocurrent signal was observed.

3.4. Enhancement effect of PAniHs on PTB7–Th

For investigating enhancement effect of PAniHs on PTB7–Th, the transient photocurrent responses of PEC biosensors modified by

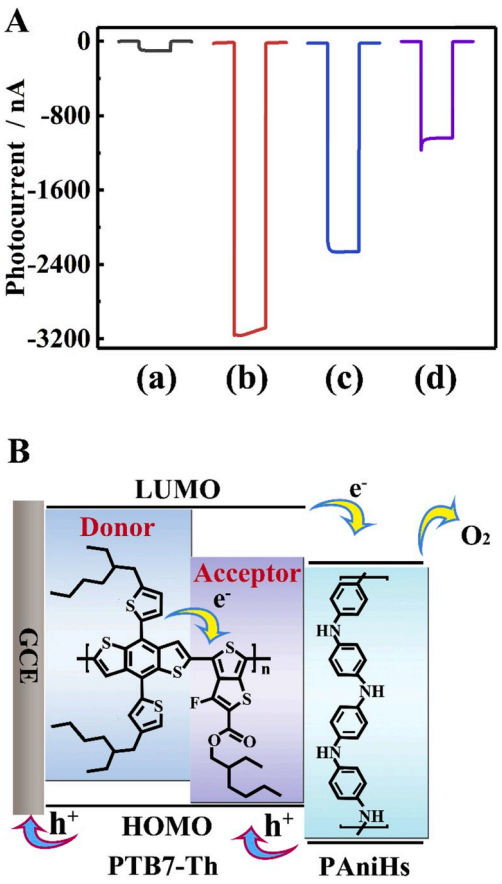

Fig. 3. (A) Photocurrent responses of different modified PEC biosensors in Tris–HCl buffer (10 mM, pH 7.4): (a) PAniHs/GCE, (b) PTB7–Th/PAniHs/GCE, (c) XOD/PTB7–Th/PAniHs/GCE, (d) XOD/PTB7–Th/PAniHs/GCE with the addition of 10 μM guanine. (B) Schematic diagrams of the photocurrent generation mechanism, LUMO denotes lowest unoccupied molecular orbital, HUMO represents highest occupied molecular orbital.

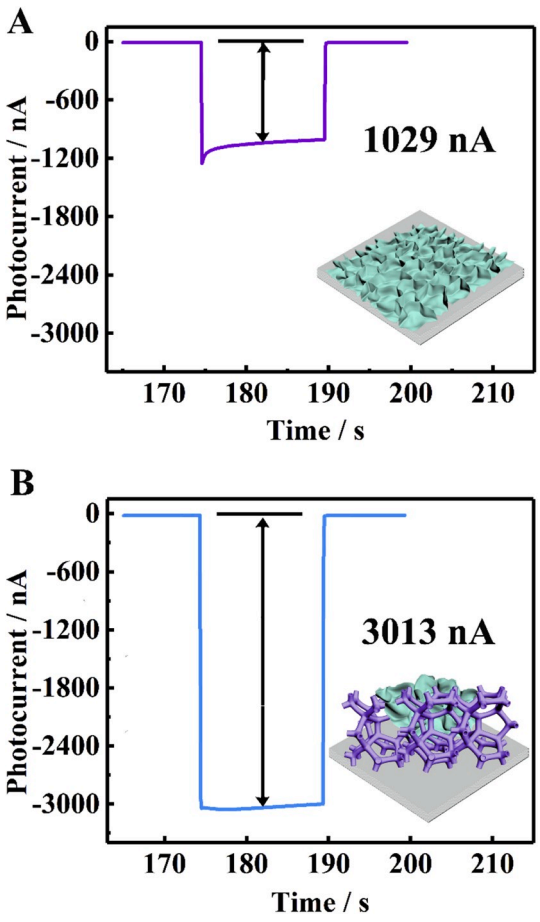

Fig. 4. Photocurrent responses of (A) PTB7–Th/GCE and (B) PTB7–Th/PAniHs/GCE in Tris–HCl buffer (10 mM, pH 7.4).

different photocurrent materials were compared. As shown in Fig. 4A, the spike appeared once the light turned on, while quickly decayed to relatively steady level within 1.0 s. The electron–hole pairs stacked on the surface of electrode rather than immediately transferred to the electron acceptor, so that the electron–hole recombination process predominated, leading to rapid decay of the initial signal. Significantly, compared with the PTB7–Th/GCE, the introduction of PAniHs significantly increased the photocurrent response (Fig. 4B), since PAniHs can serve as a signal enhancer to reduce electron–hole recombination, as well as a carrier of photoelectrical materials to enhance the light absorption.

3.5. Analytical performances

By coupling the XOD−guanine process with O_2−sensitive photocathode, different concentrations of guanine were tested under optimal conditions (Fig. S4). As depicted in Fig. 5A, the photocurrent response gradually decreased with the increase of guanine, which is caused by the competitive consumption of the dissolved oxygen between the photocathode material and the XOD. In addition, this biosensor achieved a good linear relationship between photocurrent intensity and guanine concentration in the range from 0.1 to 80 μM (Fig. 5B, inset). The corresponding linear regression equation is I (nA) = −1.2076 + 1.2361c (μM) with the regression coefficient of 0.9968. Moreover, the PTB7–Th/PAniHs photocathodic biosensor showed a good detection limit of 0.02 μM ($3S_b/m$, where m and S_b denote the slope of the linear regression equation and the relative standard deviation of the blank sample, respectively), comparable to some reported works (Table S1).

The selectivity of the XOD/PTB7–Th/PAniHs/GCE biosensor was further systematically evaluated through some possible interfering species. Hitherto, a mass of reported works introduced electron donors, such as ascorbic acid, dopamine and hydrogen peroxide, to scavenge the photogenerated holes for reducing the recombination of electron−hole pairs (Zang et al., 2017; Zhuang et al., 2015). Thus, we selected these electron donors to assess the anti–interference capability of this biosensor. In addition, common amino acids including histidine and arginine have been introduced to investigate the specificity of XOD. The results show that even if the concentration of foreign substances is 50 times of the target concentration, the PEC signal change caused by the substances can be ignored (Fig. 5C). Therefore, the XOD/PTB7–Th/-PAniHs/GCE sensing platform had a satisfactory selectivity for guanine detection. The satisfactory selectivity of this biosensor should be ascribed to the following reasons. Firstly, the XOD is inherently specific to guanine and catalyzes the production of uric acid from guanine (Zhao et al., 2017). Moreover, the cathodic photoelectrode possesses excellent anti–interference capability to reductive substances (Song et al., 2018; Zhang et al., 2018b). Additionally, consecutive off-on-off light irradiation test was conducted to assess the stability of XOD/PTB7–Th/PAniHs/GCE biosensor. The change of cathodic photocurrent was not obvious, and the relative standard deviation (RSD) was calculated to be 1.73% (Fig. 5D). We also investigated the stability of XOD/PTB7–Th/-PAniHs/GCE biosensor for detection of guanine by consecutive off-on-off light irradiation test. The relative standard deviation (RSD) of the cathodic photocurrent was calculated to be 5.18% (Fig. S5). In addition, the long-term stability of the proposed biosensor was evaluated by storing the biosensor at 4 °C and measured every two days

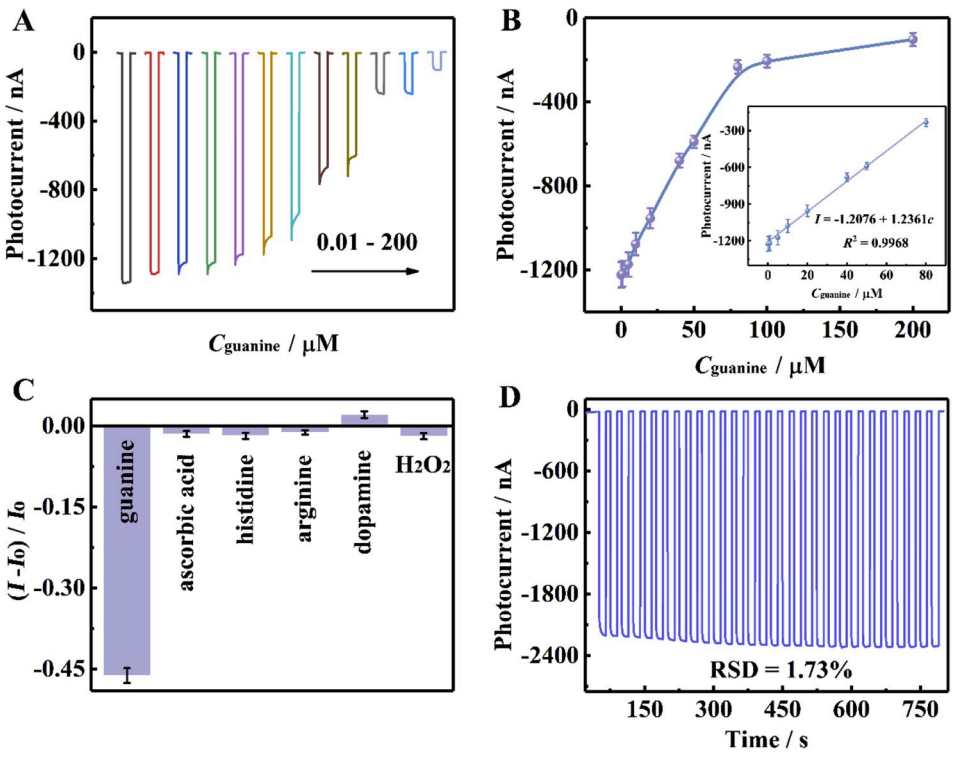

Fig. 5. (A) Photocurrent intensity of the PTB7–Th/PAniHs photocathodic biosensor toward guanine. (B) Relationship between photocurrent response and the concentration of guanine in the range from 0.01 to 200 μM and the corresponding calibration curve in the range from 0.1 to 80 μM (inset). (C) Specificity of the proposed biosensor toward 5 μM guanine, 50 μM possible interfering species including ascorbic acid, histidine, arginine, dopamine and H_2O_2. (D) Stability of the proposed biosensor in Tris–HCl buffer (10 mM, pH 7.4).

(Fig. S6). These findings demonstrated that the photocathodic biosensor displayed favorable stability.

3.6. Practical application

For evaluating the potential performance of the 3D PTB7–Th/PAniHs photosystem in practical samples, the commercial Aciclovir tablets were determined by using the proposed biosensor. The samples spiked with different concentrations of guanine were detected and the measured concentrations of guanine were calculated with the regression equation shown in Fig. 5B. As summarized in Table S2, the recovery values of the recovery experiments ranged from 91.0 to 108.8%, revealing the potential practicality of the proposed biosensor in real samples.

4. Conclusions

In summary, an innovative 3D PTB7–Th/PAniHs biosensor was successfully constructed, characterized, and applied for sensitive photocathodic bioanalysis. Because of the unique characteristics of the 3D PAniHs, such as excellent electronic transmission capability, high loading amounts, good biocompatibility as well as promoted diffusion kinetics for water–soluble matter and electrons, the developed PTB7–Th/PAniHs biosensor not only exhibited greatly enhanced initial PEC signal, but also can be used as a platform for biomolecule immobilization. Exemplified by the XOD–catalytic conversion of guanine, this biosensor showed good performance in guanine detection, which may offer a common basis for versatile photoelectrochemical enzymatic bioanalysis. Moreover, we envision that this work not only presents a new avenue for enhancing the photoelectric conversion efficiency of photoactive materials, but also paves the way for the future advancement of environmental–friendly conductive hydrogel materials in PEC bioanalysis.

Declaration of competing interest

The authors declare that they have no known competing financial interests or personal relationships that could have appeared to influence the work reported in this paper.

CRediT authorship contribution statement

Min Qing: Conceptualization, Methodology, Investigation, Formal analysis, Software, Writing - original draft. **Sheng Liang Chen:** Investigation, Validation. **Lei Han:** Investigation, Software. **Yu Zhu Yang:** Formal analysis, Data curation. **Hong Qun Luo:** Conceptualization, Resources, Project administration, Writing - review & editing. **Nian Bing Li:** Supervision, Project administration, Data curation, Funding acquisition.

Acknowledgments

This work was supported by the National Natural Science Foundation of China (No. 21675131), the Natural Science Foundation of Chongqing (CSTC–2015jcyjB50001).

Appendix A. Supplementary data

Supplementary data to this article can be found online at https://doi.org/10.1016/j.bios.2020.112179.

References

Cho, S., Seo, J.H., Kim, G.H., Kim, J.Y., Woo, H.Y., 2012. J. Mater. Chem. 22, 21238–21241.
Dong, X.X., Shi, Z.L., Xu, C.X., Yang, C., Chen, F., Lei, M.L., Wang, J.J., Cui, Q.N., 2020. Biosens. Bioelectron. 149, 111843.
Fan, Y.Y., Ma, W.G., Han, D.X., Gan, S.Y., Dong, X.D., Niu, L., 2015. Adv. Mater. 27, 3767–3773.
Fu, L.Y., Yan, L., Wang, G.R., Ren, H., Jin, L., 2019. Talanta 193, 161–167.
Gao, Y.S., Xu, J.K., Lu, L.M., Wu, L.P., Zhang, K.X., Nie, T., Zhu, X.F., Wu, Y., 2014. Biosens. Bioelectron. 62, 261–267.
Hao, N., Zhang, X., Zhou, Z., Qian, J., Liu, Q., Chen, S.B., Zhang, Y., Wang, K., 2017. Sens. Actuators, B 250, 476–483.
Jiang, W.J., Luo, W.J., Zong, R.L., Yao, W.Q., Li, Z.P., Zhu, Y.F., 2016. Small 12, 4370–4378.

Lee, K., Cho, S., Heum Park, S., Heeger, A.J., Lee, C.W., Lee, S.H., 2006. Nature 441, 65–68.
Li, J., Gao, X., Liu, B., Feng, Q.L., Li, X.B., Huang, M.Y., Liu, Z.F., Zhang, J., Tung, C.H., Wu, L.Z., 2016. J. Am. Chem. Soc. 138, 3954–3957.
Li, L.L., Wang, Y.Q., Pan, L.J., Shi, Y., Cheng, W., Shi, Y., Yu, G.H., 2015. Nano Lett. 15, 1146–1151.
Li, M.J., Tian, X., Liang, W.B., Yuan, R., Chai, Y.Q., 2018. Anal. Chem. 90, 14521–14526.
Liao, S.H., Jhuo, H.J., Cheng, Y.S., Chen, S.A., 2013. Adv. Mater. 25, 4766–4771.
Mahshid, S.S., Camiré, S., Ricci, F., Vallée–Bélisle, A., 2015. J. Am. Chem. Soc. 137, 15596–15599.
Ng, K.L., Khor, S.M., 2017. Anal. Chem. 89, 10004–10012.
Pan, L.J., Yu, G.H., Zhai, D.Y., Lee, H.R., Zhao, W.T., Liu, N., Wang, H.L., Tee, B.C.K., Shi, Y., Cui, Y., Bao, Z.N., 2012. Proc. Natl. Acad. Sci. U.S.A. 109, 9287.
Qiu, B.C., Xing, M.Y., Zhang, J.L., 2018. Chem. Soc. Rev. 47, 2165–2216.
Sayresmith, N.A., Saminathan, A., Sailer, J.K., Patberg, S.M., Sandor, K., Krishnan, Y., Walter, M.G., 2019. J. Am. Chem. Soc. 141, 18780–18790.
Shen, Q.M., Han, L., Fan, G.C., Zhang, J.R., Jiang, L.P., Zhu, J.J., 2015. Anal. Chem. 87, 4949–4956.
Shi, X.M., Wang, C.D., Zhu, Y.C., Zhao, W.W., Yu, X.D., Xu, J.J., Chen, H.Y., 2018. Anal. Chem. 90, 9687–9690.
Song, Z., Fan, G.C., Li, Z.M., Gao, F.X., Luo, X.L., 2018. Anal. Chem. 90, 10681–10687.
Tu, W.W., Cao, H.J., Zhang, L., Bao, J.C., Liu, X.H., Dai, Z.H., 2016. Anal. Chem. 88, 10459–10465.
Vilian, A.T.E., Kim, W., Park, B., Oh, S.Y., Kim, T., Huh, Y.S., Hwangbo, C.K., Han, Y.K., 2019. Biosens. Bioelectron. 142, 111549.
Wang, L.F., Zhu, W.Q., Lu, W.B., Shi, L.N., Wang, R., Pang, R.X., Cao, Y.Y., Wang, F., Xu, X.H., 2019. Biosens. Bioelectron. 142, 111577.
Wei, J., Chang, W.D., Qileng, A., Liu, W.P., Zhang, Y., Rong, S.Y., Lei, H.T., Liu, Y.J., 2018. Anal. Chem. 90, 9606–9613.
Wei, Q.X., Wang, C., Zhou, X., Wu, T., Wang, Y.Y., Li, C.Y., Yang, N.J., 2019. Biosens. Bioelectron. 142, 111540.
Wu, G., Li, L., Li, J.H., Xu, B.Q., 2006. J. Power Sources 155, 118–127.
Xu, L.H., Li, J.j., Zeng, H.B., Zhang, X.J., Cosnier, S., Marks, R.S., Shan, D., 2019a. Biosens. Bioelectron. 143, 111601.
Xu, Y.T., Yu, S.Y., Zhu, Y.C., Fan, G.C., Han, D.M., Qu, P., Zhao, W.W., 2019b. TrAC Trends Anal. Chem. (Reference Ed.) 114, 81–88.
Xue, J., Zhang, L.N., Gao, C.M., Zhu, P.H., Yu, J.H., 2019. Biosens. Bioelectron. 133, 1–7.
Ye, C., Wang, M.Q., Gao, Z.F., Zhang, Y., Lei, J.L., Luo, H.Q., Li, N.B., 2016. Anal. Chem. 88, 11444–11449.
Zang, Y., Lei, J.P., Ju, H.X., 2017. Biosens. Bioelectron. 96, 8–16.
Zang, Y., Lei, J.P., Zhang, L., Ju, H.X., 2014. Anal. Chem. 86, 12362–12368.
Zhang, G.Y., Shan, D., Dong, H.F., Cosnier, S., Al–Ghanim, K.A., Ahmad, Z., Mahboob, S., Zhang, X.J., 2018a. Anal. Chem. 90, 12284–12291.
Zhang, H.W., Hu, X.B., Qin, Y., Jin, Z.H., Zhang, X.W., Liu, Y.L., Huang, W.H., 2019. Anal. Chem. 91, 4838–4844.
Zhang, N., Ruan, Y.F., Zhang, L.B., Zhao, W.W., Xu, J.J., Chen, H.Y., 2018b. Anal. Chem. 90, 2341–2347.
Zhao, W.W., Xu, J.J., Chen, H.Y., 2017. Biosens. Bioelectron. 92, 294–304.
Zheng, Y.N., Liang, W.B., Xiong, C.Y., Yuan, Y.L., Chai, Y.Q., Yuan, R., 2016. Anal. Chem. 88, 8698–8705.
Zhuang, J.Y., Tang, D.Y., Lai, W.Q., Xu, M.D., Tang, D.P., 2015. Anal. Chem. 87, 9473–9480.